Journal of Photochemistry and Photobiology A: Chemistry 214 (2010) 1–9

Contents lists available at ScienceDirect

Journal of Photochemistry and Photobiology A: Chemistry

journal homepage: www.elsevier.com/locate/jphotochem

Bacterial inactivation kinetics, regrowth and synergistic competition in a photocatalytic disinfection system using anatase titanate nanofiber catalyst

Meng Nan Chong [a,b], Bo Jin [a,b,c,*], Huaiyong Zhu [d], Chris Saint [b,c]

[a] School of Chemical Engineering, The University of Adelaide, 5005 Adelaide, Australia
[b] Schools of Earth and Environmental Sciences, The University of Adelaide, 5005 Adelaide, Australia
[c] Australian Water Quality Centre, South Australian Water Corporation, 5000 Adelaide, Australia
[d] School of Physical and Chemical Sciences, Queensland University of Technology, Brisbane QLD 4001, Australia

ARTICLE INFO

Article history:
Received 7 September 2009
Received in revised form 9 April 2010
Accepted 25 May 2010
Available online 4 June 2010

Keywords:
TiO_2
Nanofibers
Annular reactor
Photocatalysis
Bacterial inactivation
E. coli
Post-disinfection
Fenton reaction
Synergistic competition

ABSTRACT

This work studied the inactivation kinetics, bacterial regrowth and synergistic competition in the photocatalytic disinfection of a sewage isolated *Escherichia coli* (ATCC 11775) in an annular slurry photoreactor (ASP) system using anatase titanate nanofibers catalyst (TNC). The inactivation performance and disinfection kinetics of the TNC–ASP system were investigated with respect to operation conditions: TNC loading, pH, aeration rate and inoculums size. At the optimum conditions, a 99.999% inactivation of 7×10^6 CFU mL^{-1} *E. coli* was achieved in 60 min. The modified Hom model was used to perfectly-fit the sigmoid-shaped disinfection kinetic profile. The residual disinfecting effect was evaluated by post-irradiation Fenton reaction. It was found that the 1.0 mg L^{-1} Fe^{2+} in conjunction with low chemical oxygen demand (COD) was able to initiate the post-photocatalytic Fenton reaction, where substantial bacterial regrowth was suppressed after 24 h treatment. Studies on the synergistic effect of COD concentration on the inactivation and the bacterial regrowth potential revealed that the *E. coli* could regrowth at a COD concentration over 16 mg L^{-1}. Thus, significant removal of COD has to be ensured in a photocatalytic disinfection process to successfully maintain the biostability of the treated water.

1. Introduction

The use of photocatalytic technology to eliminate trace organic pollutants in water treatment process has been well-documented [1–11]. When semiconductor titanium dioxide (TiO_2) is excited with photon energy greater or equal to its bandgap energy E_b (<385 nm), electron–hole pairs will be generated in TiO_2. It was reported that the presence of surface adsorbed hydroxyl groups is indispensable in the generation of reactive hydroxyl radicals ($OH^\bullet$) from the direct valence band (VB) hole oxidation [1–8]. To ensure the prolonged availability of VB holes, oxygen is required to capture the excited conduction band electrons through the formation of superoxide ions ($O_2^{\bullet -}$) and thus, further prevent the recombination of electron–hole pairs [9]. The presence of other reactive oxygen species (ROS) during the photocatalytic reaction in an aqueous environment, such as hydrogen peroxide (H_2O_2) and singlet oxygen, has also been reported [9]. In the absence of oxygen or other electron acceptors, no photocatalytic reaction occurs due to the rapid recombination of electron–hole pairs. The detailed photochemical reactions on the TiO_2 surface during photocatalysis have been discussed in numerous literatures [9–11].

In recent years, the emergence of toxic disinfection by-products (DBPs) from water chlorination has been of major environmental and public health concern [12–14]. Prominent DBPs such as haloacetic acids and trihalomethanes can cause congenital cardiac defects in human beings, if their concentration is higher than 60 or 80 ppb, respectively [14]. Removal of such DBPs in a cost-effective and sustainable manner is keenly sought, owing to their persistent nature that might penetrate through to the end-user. Considering the growth in treatment of recycled wastewater for domestic utilisation, there is a need to find a sustainable water disinfection technology to replace chlorination, so as to avoid the formation of DBPs. To date, chlorination is still the preferred disinfection method owing to its cost-effective removal of microorganisms and the ability to maintain residual free-chlorine that prevents further bacterial regrowth [15,16].

Since the first application of TiO_2 photocatalyst under UV irradiation for microbial inactivation by Matsunaga et al. in 1985,

* Corresponding author at: Schools of Earth and Environmental Sciences, The University of Adelaide, 5005 Adelaide, Australia. Tel.: +61 8 8303 7056; fax: +61 8 8303 6222.
E-mail address: bo.jin@adelaide.edu.au (B. Jin).

1010-6030/$ – see front matter © 2010 Elsevier B.V. All rights reserved.
doi:10.1016/j.jphotochem.2010.05.018

many preliminary investigations were performed to examine the possibility of using photocatalytic technology for water disinfection [17]. A wide range of microbial types, from coliforms, viruses, bacteria, cysts, fungi, algae and protozoa have been successfully inactivated using photocatalytic disinfection [18–20]. Surprisingly, very few cases were reported for a pilot or large scale photocatalytic disinfection process except those reported by Rincón and Pulgarin [16]. This was largely attributed to the difficulty in downstream process for the recovery of the powder photocatalysts, such as commercial Degussa P-25 TiO_2, and thus limited its industrial application [21–23]. Numerous engineering solutions have been adopted to enhance the feasibility of photocatalytic disinfection technology. One of the prominent solutions is to utilise an inert carrier for the immobilisation of TiO_2 particles. Different inert carriers, such as optical fibers, clay materials and magnetic core TiO_2 particles have been previously investigated [24–31].

The use of photocatalytic disinfection technology for water treatment has been reported to exhibit a lesser extent of residual disinfecting effect (RDE) against the chlorination [32–34]. The RDE was restricted by the nature of the $OH^{\bullet}$ radicals, which usually have a short half-life in the water environment. Wist et al. [15] reported that there is a drastic increase in the culturable *E. coli* cells in the crude river water sample in the subsequent 24 h after UV irradiation. Similar bacterial regrowth problems were observed by Rincón and Pulgarin [32] after 48 h of UV irradiation. To enhance the RDE of photocatalytic disinfection, a consecutive illuminated TiO_2 photocatalysis and post-irradiation Fenton reaction were proposed [33]. The ROS of H_2O_2 was the primary species that is responsible for initiating the dark Fenton reaction, together with the presence of trace transition metals (i.e. Fe, Mn or Cu). The residual H_2O_2 from the illuminated TiO_2 reaction phase will be periodically reverted into $OH^{\bullet}$ with the aid of such transition metals, preventing any bacterial regrowth [33]. In this instance, it is important to stress that the targeted water quality constitutes one of the major suppressant to diminish the RDE of the photocatalytic disinfection. It is thus, imperative to understand the extent of the dark Fenton reaction for enhanced RDE on photocatalytic water disinfection.

In this study, we first revealed the superiority of a recently developed anatase titanate nanofiber catalyst (TNC) for the photocatalytic disinfection of a sewage isolated *E. coli* (ATCC 11775) strain under UVA irradiation ($\lambda < 380$ nm). We have reported the photocatalytic degradation of organics over the TNC surface and its particle recovery [35]. The TNC was found to have a competitive separation edge over the commercial Degussa P-25 TiO_2 with enhanced surface mass transfer for both the adsorbed reactants and desorbed photocatalyzed products [35]. The influence of operation parameters of the ASP system on the bacterial inactivation and irradiation time were investigated. These parameters include the TNC loading, pH, aeration rate and bacterial inoculums size. The sewage-isolated *E. coli* strain was used as an indicator microorganism for faecal contamination and microbiological standard to measure against the photocatalytic treatment efficiency. So far, *E. coli* is the most widely used microbial standard for studying water disinfection and thus, considered appropriate for comparison with other studies. Currently, it is also utilised as a key indicator organism for the effective disinfection of wastewater. We used the experimental data and disinfection kinetic model for comparison of photocatalytic disinfection efficiency. Subsequently, the RDE of the TNC–ASP system was evaluated by the post-irradiation Fenton reaction against different Fe^{2+} concentrations, with the presence of glucose as the organic carbon source. The synergistic effect of the chemical oxygen demand (COD) on the photocatalytic inactivation of the *E. coli* and its bacterial regrowth potential (BRP) were investigated.

2. Experimental

2.1. Materials

Ferrous sulphate ($FeSO_4{\cdot}7H_2O$, Analar grade, BDH Chemicals, England), D(+)-glucose ($C_6H_{12}O_6$, BDH VWR, England) and digestion solution for COD 0–150 ppm range (Hach, USA) were used as received. Hydrochloric acid (HCl) (Labserv Pronalys, Australia) and sodium hydroxide (NaOH) (Analar grade, BDH Chemicals, England) were prepared to a desired concentration by the addition of Milli-Q water obtained from Barnstead Nanopure Barnstead ion exchange water system with 18.2 MΩ-cm resistivity.

The *anatase titanate nanofiber catalyst* (TNC) was previously synthesized through a hydrothermal reaction between concentrated NaOH and TiO_2 and a post-synthesis ion exchange with HCl solution [36,37]. Specifically, 3 g of anatase particles (~325 mesh from Aldrich) was mixed with 80 mL of 10 M NaOH. The resultant suspension was sonicated for 30 min and transferred into a PTFE container for autoclaving. The autoclave was maintained at a hydrothermal temperature of 180 °C for 48 h. The precipitate (sodium titanate nanofiber) was recovered, washed with distilled water (to remove excess NaOH) and finally sodium ions in the titanate nanofibers were exchanged with H^+ ions (using a 0.1 M HCl solution) to produce hydrogen titanate nanofibers. These products were repeatedly washed with distilled water until pH ~7 was reached. The hydrogen titanate product was dried at 80 °C for 12 h and then calcined at 700 °C for 3 h to yield anatase nanofibers.

2.2. Annular slurry photoreactor system

A previously developed stainless steel-lined ASP column was used as a photo-disinfection reactor in this study [5,35]. The ASP was operated as a three-phase bubble column reactor, where the TNC fibrils were dispersed in the targeted water. The lower-end of the ASP was fabricated with a detachable conical bottom free of a reaction dead zone, making it easy for cleaning and maintenance. A 45-μm air sparger was fitted to the detachable conical bottom to provide homogeneous bubble distribution for agitation, mixing and aeration for the photocatalytic reaction. The light configuration in the ASP was designed in such a way, where additional light could be placed within the central quartz core. In this study, an UVA black light of 8W (NEC, Holland) was fitted annularly within the quartz thimble to prevent direct contact with the reaction fluid, while allowing optimal UV transmission for excitation of the suspended TNC fibrils. It should be stressed that the UVA light used in this study was purely for the photonic excitation of the TNC alone. Unlike the germicidal UVC light with high-end UV electromagnetic spectrum (i.e. 4.43–12.4 eV), the associated UV energy for such UVA is significantly lower (i.e. 3.10–3.94 eV) and will not cause substantial bacterial inactivation [16]. The wavelength range of UVA light lies in the range of 315–400 nm, which is close to solar irradiation. Samples were collected from the four-descended level sampling ports. Electronic probes and meters for in situ data logging of pH, dissolved oxygen (DO) and temperature (TPS, Australia) were connected to the reactor. The operating temperature for the ASP system was kept at room temperature of 25 °C during the experiments. A detailed design of the ASP and the whole experimental set up are shown in Fig. 1.

2.3. Preparation of bacterial strain and water samples

A sewage-isolated *E. coli* strain (ATCC 11775) was used as an indicator microorganism for faecal contamination and microbial standard to evaluate the inactivation performance and disinfection efficiency.

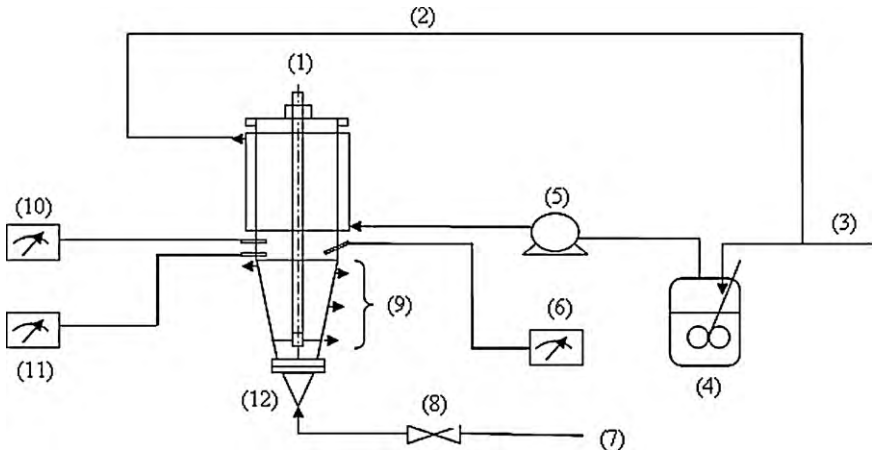

Fig. 1. Experimental set-up for the annular slurry photoreactor system: (1) UV light, (2) recirculation water line, (3) fresh cool water line, (4) cooling water vessel, (5) cooling water pump, (6) temperature meter, (7) compressed air supply line, (8) compressed air regulation valve, (9) sampling ports, (10) pH meter, (11) dissolved oxygen meter, and (12) photoreactor.

The ASP was first filled with 1.5 L of bacterial suspension of known cell number for each batch run. A 50 mL fresh liquid culture was prepared by inoculation in a tryptone soy broth media (TSB) (Oxoid, England) and was followed by incubation at 35 °C for 19 h in a rotary shaker at 50 rpm. The final bacterial count after 19 h incubation was determined to be 9×10^9 CFU mL^{-1}. To prepare the bacterial suspensions, 1.5 L of phosphate buffered saline (PBS) solution prepared using Nanopure Water of 18.2 MΩ cm resistivity was inoculated accordingly. The use of PBS is to prevent sudden osmotic shock to the bacteria, so as to maintain the bacterial numbers for accurate dilution purposes. Subsequently, the initial bacterial density was heterotrophic plate counted (HPC) using standard procedures [38].

Prior to the batch disinfection trial, TNC at a given concentration was added to the bacterial suspension in the ASP and further homogenized in the dark for 30 min under constant aeration. The UVA light was turned on after the homogenisation period at $t = 0$ min and the aeration were allowed to run continuously up to 120 min. The sampling was conducted every 10 min up to 40 min, and thereafter every 20 min up to 120 min. The determination of the *E. coli* was carried out following a standard serial dilution procedure and every sample was HPC duplicately in the prepared plate count agar (PCA) (Merck, Germany). The PCA plates were incubated at 35 °C for 24 h before final cell counting. The normalised fraction of bacterial survivor against irradiation time curves was plotted for disinfection kinetic analysis. Each photo-disinfection experiments were then repeated for standard experimental verification and error analysis.

For the RDE experiments, we added a fixed amount of glucose to the pure water and adjusted the pH. A specific amount of Fe^{2+} was also added to the ASP before the experiment. The bacterial suspension was prepared in the same procedures as described previously. After UV irradiation for 120 min, 150 mL of the treated water sample were charged into a 250 mL flask. The flask was incubated at 35 °C in the orbital shaker incubator at 150 rpm for 24 h. The treated water sample was subjected to HPC to monitor the efficacy of post-irradiation Fenton reaction. Similarly, each analysis was repeated for standard experimental replication and error analysis.

2.4. Water sample analysis

Organic carbon, referred as COD, during the entire illuminated TNC reaction phase in the TNC–ASP was monitored using a COD measurement kit (Hach, United States), which comprises of COD digestion solution, Hach DRB 200 digestion chamber and Hach DR890 COD calorimeter. Two milliliters of the treated water sample after the UVA irradiation was added into the digestion solution. The digestion solution was then subjected to the digestion chamber at 150 °C for 120 min. After digestion, the solution was allowed to cool down prior to the COD measurements using the calorimeter. In addition, 100 μL of the supernatant was then filtered through a 0.22 μm membrane for glucose analysis by HPLC. The HPLC analysis used a ROA Organic Acid Column (Phenomenex, 300 × 7.8, Varian, CA, USA) and a refractive index detector (Model 350, Varian). The mobile phase was 4 mM H_2SO_4 at a flow rate of 0.6 mL min^{-1} and the column temperature was 50 °C.

3. Results and discussion

3.1. Effect of TNC loading

The influence of photocatalyst loadings on microbial inactivation in different photocatalytic systems has been reported [39]. Experiments were carried out in the TNC–ASP system using TNC at a loading range of 0.25–2.0 g L^{-1}. Two control experiments without either TNC or UVA irradiation were also tested. Fig. 2 shows the normalised plot of enumerated *E. coli* cells against UVA irradiation time. The TNC showed no inactivation activity on the *E. coli* in the dark control experiment. A small fraction of the *E. coli* was inactivated under the UVA irradiation without TNC. Since the UVA radiation (320–400 nm) is the least energetic fraction of the UV spectra, the radiation-induced cell damage to the bacterial cell is usually insignificant owing to the absence of direct absorption by the sensitive cell components [16]. It was reported that the photokilling by UVA irradiation should be well-mediated by sensitizers, such as TiO_2, to achieve greater bacterial cell damage [16].

When 0.25 g L^{-1} TNC was added (Fig. 2) as the sensitizer in inducing the formation of chemical intermediates during the irradiation period, such as $OH^{\bullet}$, $O_2^{\bullet -}$ and H_2O_2, significant enhancement in *E. coli* inactivation was observed. An inactivation level of 99.999% was easily attained within 120 min irradiation, resulting in a significant 5-fold enhancement in *E. coli* inactivation higher than the control experiment with UVA irradiation alone. Using 0.5 g L^{-1} TNC, the irradiation time taken to achieve 99.999% of bacterial inactivation was reduced to 100 min, while a shorter irradiation time of 80 min was needed as the TNC loading increased to 1.0 g L^{-1}. However, a further increase in TNC loadings to 2.0 g L^{-1} resulted in a significant prolongation of irradiation time required to achieve similar bacterial inactivation levels. We found that at longer irra-

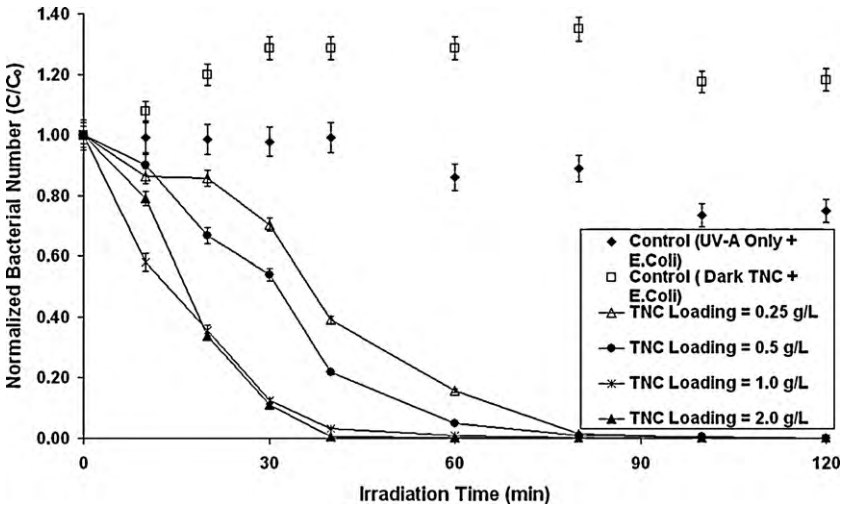

Fig. 2. Effect of TNC loading on the photocatalytic inactivation of *E. coli* at average initial bacterial population of 7×10^6 CFU mL^{-1}.

diation time, such as 360 min had limited impact on the bacterial inactivation level.

Ochuma et al. [8] found that an increase in the catalyst particle concentration in a photoreactor results in increasing the light source extinction coefficient, and subsequently reducing the reaction efficiency. This is owing to the attenuation of light intensity across the annulus zone and rapid increase in light absorption and scattering phenomena that hinder the photocatalytic inactivation to proceed at a high rate. As a consequence of such TNC saturation within the annulus reaction zone, a non-linear inactivation profile with strong tailing characteristics was observed with increasing TNC loadings. This was strongly evidenced from the long irradiation time required to achieve 99.999% inactivation if the TNC loading was doubled from 1.0 to 2.0 g L^{-1}. We believe that the efficiency of the photocatalytic disinfection in the ASP is a strong function of the annulus width, where a significant reduction in the annulus results in greater disinfection efficiency and less bacterial tailing characteristic. Wider annulus gap, together with low light intensity and high TNC loadings can affect extinction co-efficiency and result in decreasing photon contact with *E. coli* adhered to the reactor wall. Thus, it can be concluded that the saturation TNC loading in the ASP system is at 1.0 g L^{-1} for the effective disinfection. The subsequent investigations were carried out at the saturated TNC loading of 1.0 g L^{-1}.

3.2. Effect of pH

The impact of pH on TiO_2 surface charge and its photo-oxidation performance for effective surface adsorption and reaction with organics and bacteria has been well-documented [5–8,40,41]. In our previous study, we found that the point of zero charge (PZC) of TNC is 4.6, which is slightly lower than the Degussa P25 TiO_2 of 5.6–6.8 [35]. To elucidate the effects of pH in the photocatalytic inactivation of *E. coli* by TNC, the variation in pH 4.0–9.0 in the TNC–ASP was investigated in this study.

E. coli is a Gram-negative bacterium with the outer cell membrane covered by a lipopolysaccharide layer of 1–3 μm thickness [42]. With the slightly negatively charged surface of the *E. coli*, it is expected that the bacterial cell could induce an electrostatic attraction with TNC fibrils of surface charge lower than its PZC value. The water pH affects the surface charge density of the TNC according to the following equilibrium equations (Eqs. (1) and (2)) [40];

$$\text{pH} < \text{PZC} : \text{TiOH} + \text{H}^+ \leftrightarrow \text{TiOH}_2{}^+ \quad (1)$$

$$\text{pH} > \text{PZC} : \text{TiOH} + \text{OH}^- \leftrightarrow \text{TiO}^- + \text{H}_2\text{O} \quad (2)$$

Fig. 3 shows the effect of pH on the photocatalytic inactivation of *E. coli*. Initial pH was adjusted by dropwise addition of 0.1 M

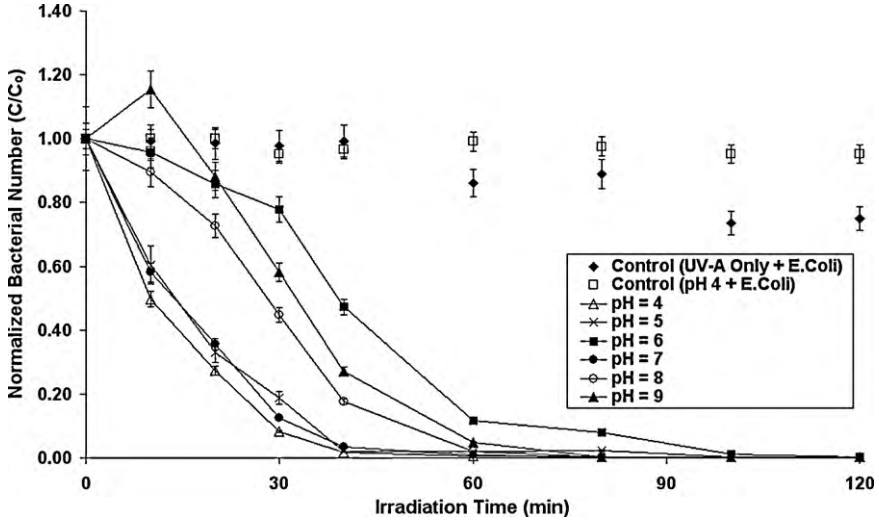

Fig. 3. Effect of pH on the photocatalytic inactivation of *E. coli* at average initial bacterial population of 7×10^6 CFU mL^{-1} and TNC loading of 1.0 g dm^{-3}.

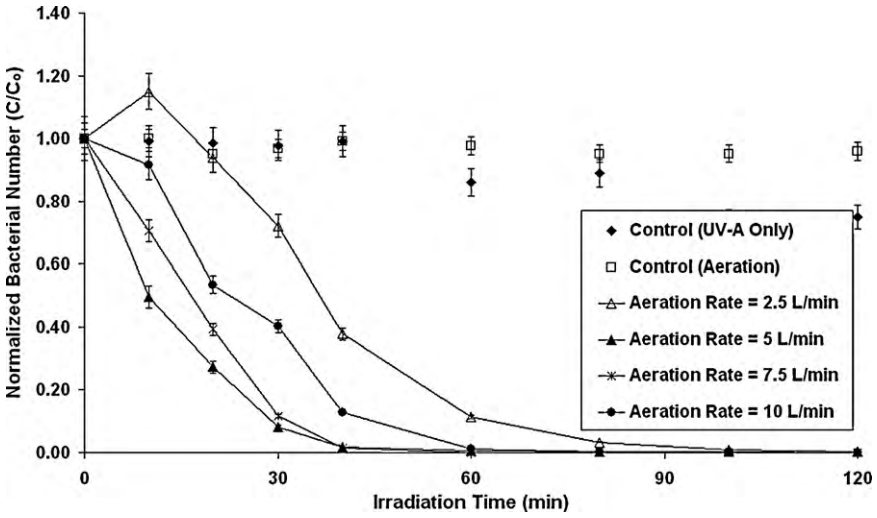

Fig. 4. Effect of delivered aeration rate in the ASP column on the photocatalytic inactivation of *E. coli* at average initial bacterial population of 7×10^6 CFU mL^{-1}, TNC loading of 1.0 g dm^{-3} and pH 4–5.

HCl and NaOH. Control experiments under UVA irradiation and pH 4.0 were conducted to measure the extent of bacterial cell lysis, as induced by the pure photolytic and cell acidification reaction, respectively. Results show that the control UVA photolytic reaction on *E. coli* contributes to an approximate 25% inactivation, while no significant destruction was observed via cell acidification at pH 4.0. Rincón and Pulgarin [40] reported similar findings where the photolytic inactivation of *E. coli* was independent of initial pH between 4.0 and 9.0.

At pH 4.0 < PZC (TNC), we found that the photocatalytic inactivation was enhanced. This may be that more *E. coli* was attracted to the positively charged TNC surface, resulting in forming dense $TiOH_2^+$ groups (Eq. (1)) that attract the bacterial cell to the TNC surface for subsequent photo-oxidation reaction. The irradiation time required to achieve 99.999% inactivation was improved to 70 min. A similar enhancement in the inactivation was observed at pH 5.0. We found that such enhancement was contributed by the TNC action alone, where slight bacterial resistance (i.e. tailing/regrowth) to TNC was not observed during the controlled acidification experiment (pH 4). Heyde and Portalier [43] found that such negligible *E. coli* reaction to acid conditions was due to the presence of an acid tolerance response in the bacterium itself, which secreted the acid-induced proteins for bacterial acid-shock protection.

It is however, interesting to note that the inactivation of *E. coli* at a slight acidic pH of 6.0 was slowed down compared to the experiment at other pH conditions. One of the possibilities is link to the growth nature of *E. coli* at pH 6.0 that overcomes the photocatalytic activity of TNC [40]. The tendency of bacterial growth at this pH range might partially reduce the rate of photocatalytic destruction on the bacterial cell. Together with the inception of electrostatic repulsion forces that avert the *E. coli* from the TNC surface at pH 6.0, this prevents the *E. coli* from the TNC surface interaction for effective photo-destruction. In short, it can be concluded that the photocatalytic inactivation by the TNC fibrils was best performed at pH 4.0–5.0. Operating the photocatalytic inactivation system at a high pH would result in prolonged photo-destruction of *E. coli* to achieve a high inactivation level. Although much justifications have been discussed in link of the *E. coli* sensibility to both low and high pH conditions, other operating issue might be neglected such as the TNC aggregation as a function of pH. All the subsequent experiments were performed at pH 4.0–5.0.

3.3. Effect of aeration rate

In this study, compressed air was used as the aeration medium to keep the TNC fibrils in suspension within the annulus core of the ASP column. Previously, we examined the effect of aeration rate on the photodegradation of anionic Congo Red dye [35]. We found that the aeration rate is a key operation parameter, which can significantly affect the mixing, dispersion or aggregation state of the catalyst particles within the ASP column.

To understand the effect of the aeration rate on the inactivation performance of the TNC–ASP system, a control experiment was performed at an aeration rate of 5 L min^{-1} without photocatalyst. Results indicate that there is no net aeration effect on the bacterial cell numbers. With this, we can conclude that there is minimal effect of aeration on the bacteria and its subsequent inactivation was solely dependent on the combined effect of UVA photolytic mediated with TNC photocatalytic activity. Fig. 4 shows the effect of the aeration rate on the inactivation of *E. coli* in the ASP column. It shows that at a low aeration rate (2.5 L min^{-1}), the photocatalytic inactivation yields sluggish kinetics with strong shoulder phenomena up to 30 min before cell destruction takes place. Such shoulder characteristic might be owing to the low volumetric generation rate of the ROS as a direct result of poor dispersion for the TNC fibrils [13,44]. We previously found that at a similar aeration rate, large amounts of TNC fibrils were sediment on the sparger plate. This indirectly reduces the amount of TNC fibrils in suspension for photon excitation, and thus the amount of active TNC for bacterial inactivation. A further increase (up to 10 L min^{-1}) in aeration rate resulted in a reduction of the photocatalytic inactivation rates. We found that the optimal aeration rate for the ASP column was 5.0 L min^{-1} with 99.999% inactivation in 60 min. A higher aeration rate (i.e. >5.0 L min^{-1}) might induce the TNC fibril aggregation, and thus reduce the total available TNC active sites for inactivation.

In addition, we performed the DO probing for its variation throughout the irradiation period. It should be noted that the correlation between the aeration rate and DO is not proportionate, with restriction from the ASP column gas hold-up and oxygen-air equilibrium. We observed that the DO profile (data not shown) was rapidly revived to a higher value after a slight drop within the initial 10 min at the saturation TNC loading of 1.0 g L^{-1}. This can be explained that the photo-destruction taking place before any microbial respiration may result in generating high concentration of the ROS. The rapid revival of the DO to its saturation level might

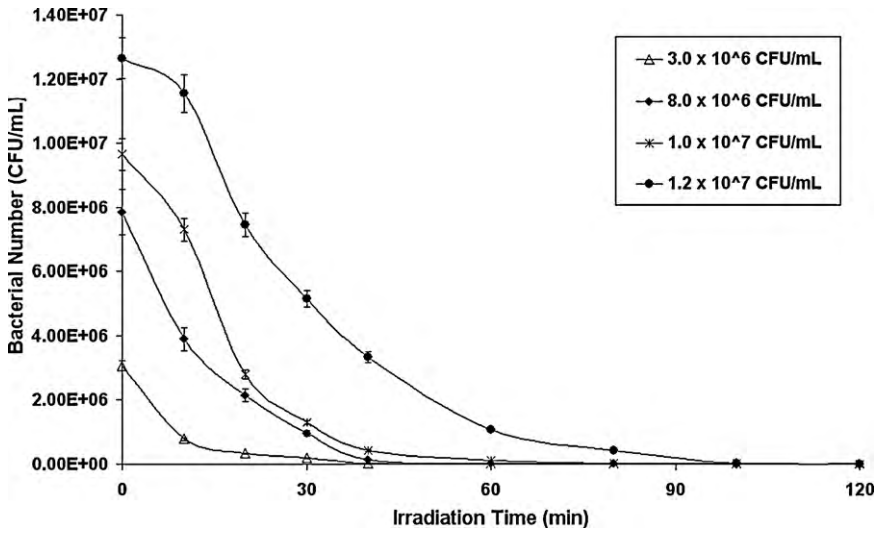

Fig. 5. Effect of bacterial population on the photocatalytic inactivation of *E. coli* under operating conditions of ASP: TNC loading of 1.0 g dm^{-3}, pH 4–5 and aeration rate of 5 dm^3 min^{-1}.

due to the performance of the ASP system, where it was operated as an open system. Also we believe that the morphology of the thin TNC fibrils (i.e. 40–100 nm) does not trap any DO within its physical structure and thus, present a promising physical structure for an efficient photocatalytic disinfection process.

3.4. Effect of bacterial population

The bacterial cell numbers may vary in a water treatment plant and thus, it is necessary to investigate the impact of initial *E. coli* numbers on the photocatalytic inactivation kinetics. Dunlop et al. [12] suggested that an increase in the initial bacterial loading enhances the interaction with the photocatalyst used and reduces the overall mass transfer limitations, resulting in a higher inactivation rate. Similar observation was reported by Pham et al. [44] during the inactivation of *Bacillus pumilus* spores in a slurry reactor.

Fig. 5 shows the effect of initial bacterial numbers on the rate of photocatalytic inactivation in the TNC–ASP system. We found that an increase in *E. coli* numbers improves the inactivation rate, as evidenced from the steeper log-linear inactivation region of the kinetics profile. Although a steeper inactivation curve was attained, the inactivation level was slightly reduced owing to the increase in water turbidity across the annulus radii. Such an improved disinfection rate was attributed to the increased collision probability between the surface-generated ROS and bacterial *E. coli* [12]. Due to the appearance of strong shoulder and tailing characteristics in the inactivation profiles, a direct comparison in the inactivation rate could not be easily made. We have compared the *E. coli* inactivation kinetics empirically by fitting with the modified Hom model and this is further discussed in the following section.

3.5. Empirical modelling of the TNC-ASP system

Bacterial inactivation modelling was attempted with the classical Chick–Watson model that conformed to a first-order relationship between the photocatalyst loading and enumerated *E. coli* [45–48]. In this study however, we found that such a linear relationship was inadequate to represent the three different regions of the photocatalytic inactivation curves in the TNC–ASP system, as shown in Fig. 5. The inactivation curve starts with (i) a lag or initial smooth decay, which is known as a "shoulder", followed by (ii) a typical log-linear inactivation region and ends with (iii) a long deceleration process at the end of the disinfection, which is known as a "tail" [13]. Cho et al. [48] attempted to use a delayed CW model with empirical lag time to represent the shoulder characteristic, but not the tailing region simultaneously.

To fit the inactivation kinetics in the TNC–ASP system, the empirical model might require three different kinetic parameters for each characteristic region. The shoulder region was justified by the cumulative damage nature of the photocatalytic treatment on the cytoplasmic membrane rather than instantly lethal [49]. This can also be viewed in terms of the slow permeation rate of the ROS, which are bounded by their short half-life, through the cell wall before inducing any irreversible damage to the bacterial cell. The tailing region was related to the competition for photocatalysis between the organic products released from the constant cell lyses [50]. Here, we used the modified Hom model for kinetic evaluation as previously used by Marugán et al. [13]. They utilised this modified Hom model to represent the photocatalytic inactivation of *E. coli* using commercial Degussa P25 TiO_2. Thus, a direct comparison could be made between the TNC fibril photocatalyst and the commercial one. Fig. 6 shows the modified Hom model fitted kinetics at the variable initial *E. coli* population. The log-linear inactivation rate constant (k_2) varied in the range of 0.053–0.098 min^{-1}. From this, we can conclude that the inactivation activity of TNC is comparable to Degussa P-25 TiO_2. Given that the TNC was found to have a competitive separation edge over the commercial Degussa P-25 TiO_2, which is difficult to be recovered for reuse, the anatase nanofibers should be considered as a potential photocatalyst for water treatment.

3.6. Influence of Fe^{2+} on the residual disinfecting effect

Previous works on photocatalytic inactivation of different microbes mostly focused on the bacterial reduction, without further monitoring the BRP of the water after photocatalytic treatment. Dunlop et al. [12] and Rincón and Pulgarin [16] investigated the dark repair mechanisms associated with the remaining bacteria during the post-irradiation period. Farr and Kogoma [51] proposed that the bacterial cells may enter a viable but non-culturable (VBNC) state when they were exposed to oxidative stress, but will be reverted to a viable state when growth conditions become favourable. To verify these propositions, we investigated the bacterial lethality of *E. coli* induced by the TNC fibrils after 120 min irradiation and the BRP in the subsequent 24 h period. Glucose (0.1 g L^{-1}) was added to the reaction water as the baseline organic

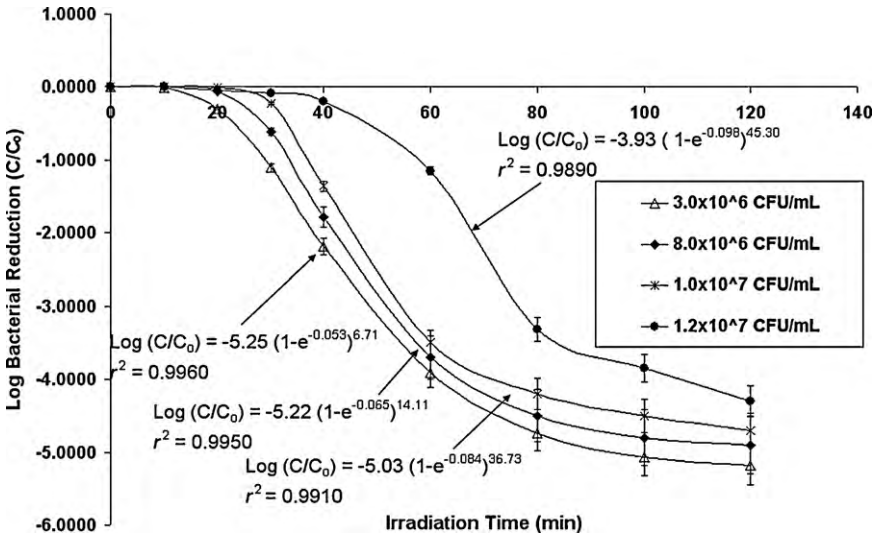

Fig. 6. Fitting of modified Hom empirical model to experimental data with different initial bacterial concentrations.

carbon source, in order to prevent the bacterial lyses from limiting nutrient conditions during the 24 h dark period. The Fe^{2+} at different concentrations was supplemented at the beginning of the experiment, in order to observe the RDE during the post-irradiation Fenton reaction. It is known that Fe^{2+} can exist in different hydrolysed forms in water, and the Fe^{2+} can dissociate H_2O_2 molecules into $OH^{\bullet}$ radicals [16]. The followings represent the chemical equilibrium of Fe^{2+} and its ferric aquacomplexes on the continuous evolution of $OH^{\bullet}$ radicals during the post-irradiation period [16]:

$$Fe^{2+} + H_2O_2 \rightarrow Fe^{3+} + OH^- + OH^{\bullet} \quad (4)$$

$$Fe^{3+} + H_2O_2 \rightarrow Fe^{2+} + HO_2^{\bullet} + H^+ \quad (5)$$

$$Fe(OH)^{2+} + h\upsilon \rightarrow Fe^{2+} + OH^{\bullet} + H^+ \quad (6)$$

Fig. 7 shows the tendency of bacterial regrowth under different experimental conditions (i.e. with/without Fe^{2+} and without glucose/TNC). Control experiments without glucose show that the *E. coli* numbers remain low during the post-irradiation period, indicating no bacterial regrowth occurs. In the control experiment with 1.0 mg L^{-1} Fe^{2+}, there was a 55% inactivation of *E. coli* found over the 120 min. After the latent period of photo-Fenton reaction, the population of *E. coli* further increased 10% from the initial culturable cell numbers. This increase in *E. coli* numbers is owing to the presence of the baseline glucose and parallel absence of the BRP-inhabitant H_2O_2 species (i.e. TNC absent) from the preceding photocatalytic reaction.

In the TNC control experiment with no Fe^{2+} added, the bacterial lethality was high in the first 120 min. There was a strong bacterial regrowth found in the subsequent 24 h dark period. In this instance, the absence of Fe^{2+} was seen to be more beneficial for bacterial regrowth than the absence of the TNC. When 0.1 mg L^{-1} Fe^{2+} was added, its inactivation kinetic profile was of more log-linear type (i.e. shoulder becomes more subtle) relative to standard TNC control experiment. A 99.995% reduction in *E. coli* was attained after the first 120 min irradiation. During the subsequent 24 h, the bacterial regrowth resulted in numbers equating to 93% of the initial *E. coli* numbers.

At higher Fe^{2+} concentrations of 0.3 and 1.0 mg L^{-1}, respectively, both the initial photo-killing rate and RDE effect becomes more prominent than the experiment using 0.1 mg L^{-1} Fe^{2+}. A more distinct sigmoid-type of inactivation profile was observed in the TNC–ASP system with more Fe^{2+} added. It can be seen that at a high concentration of Fe^{2+} (i.e. 1.0 mg L^{-1}), the sigmoidal profiles become prominent but a prolonged irradiation time is required to

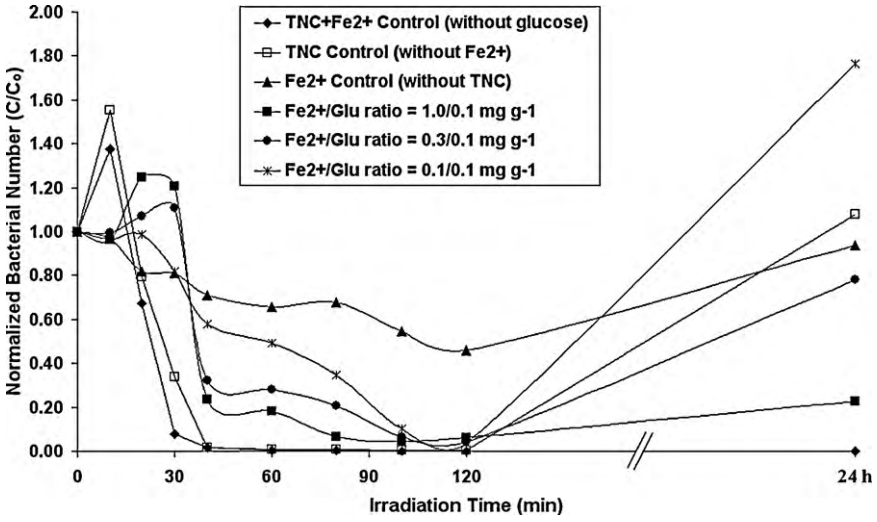

Fig. 7. Evaluation of the residual disinfecting effect of combined TNC/Fenton treatment during the subsequent 24 h under different Fe^{2+} ion concentrations. Initial glucose concentration is 100 mg.

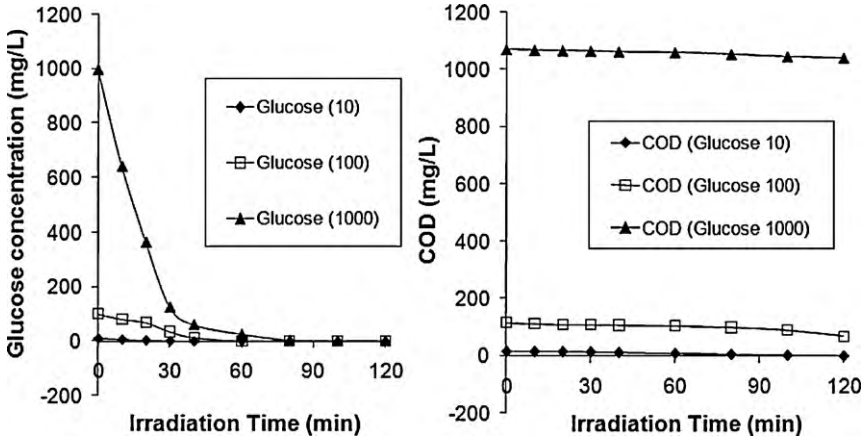

Fig. 8. Correlation between the mineralization of glucose and its corresponding COD during the photocatalytic inactivation of *E. coli* (as in Fig. 7).

achieve a similar inactivation level. As for the RDE, we found that the Fe^{2+} at a high concentration could partially suppress the bacterial regrowth during the subsequent 24 h dark period. Under this 24 h period, use of 1.0 mg L^{-1} Fe^{2+} resulted in only 20% regrowth, while a significant high bacterial regrowth of 78% was associated with using 0.3 mg L^{-1} Fe^{2+}. A high Fe^{2+} concentration may cause water colorization. The maximum Fe^{2+} concentration allowed for recycled water is 1.0 mg L^{-1}. Thus, 1.0 mg L^{-1} Fe^{2+} was used in this study in order to simulate the real water treatment conditions. One of the possibilities for such a weak RDE effect is owing to the low H_2O_2 generated during the irradiation and fast recombination with $OH^{\bullet}$ to form HO_2. It was anticipated that the addition of supplementary H_2O_2 up to 0.3 mmol L^{-1} could enhance the BRP effect of TNC, as discussed by Rincón and Pulgarin [16]. Other possibilities might be due to the presence of organic carbon, whose synergistic effects on the bacterial regrowth will be discussed in Section 3.7.

3.7. Synergistic interaction between COD and E. coli in the photocatalytic disinfection process

The presence of organic compounds in either dissolved or particulate form in the treated water might provide sufficient carbon and energy sources for bacterial regrowth [52–55]. In considering reuse of treated wastewater, the BRP in the water sources should be suppressed and the microbial population need to be lower than the standard level in the recycled water scheme. The concentrations of such organic compounds vary from different treatment plants, mainly depending on the efficiency of the water treatment process. It was reported that the COD level of treated wastewater might vary between 45 and 150 mg L^{-1}, depending on the seasonal activities of the local population [52].

We investigated the effect of organic carbon concentrations on the BRP of the treated water. Glucose at 0.01, 0.1 and 1.0 g L^{-1} were added, in order to make up different baseline COD conditions. The addition of glucose is also to verify its synergistic mineralisation during the photocatalytic treatment. With 1.0 mg L^{-1} Fe^{2+} added, the water was subjected to photocatalytic treatment for 120 min, followed by dark incubation at 35 °C for 24 h. The glucose concentration and the COD were monitored during the treatment period. The residual number of *E. coli* after the 24 h dark period was monitored using HPC.

A control experiment was performed on the glucose degradation alone in a 120 min treatment. We found that at the optimised ASP conditions, 0.1 g L^{-1} glucose was completely degraded after 120 min of photocatalytic treatment. When the experiment was repeated with the co-existence of *E. coli* suspension, a slower degradation of glucose was observed after 120 min. The COD remained at a relatively high level of 87 mg L^{-1}. Parallel interpretation of the glucose and COD suggested that the glucose molecules were photocatalyzed into other intermediate organic carbons during the 120 min of photo-oxidation. Such transition in organic carbon state indicates that the *E. coli* is more susceptible to the photo-oxidation than the simpler organic carbon molecules which are more persistent and require longer irradiation time. The existence of such intermediate organic carbons, as a direct result of photocatalytic treatment was observed to synergistically affect the bacterial regrowth.

To verify the impact of organic carbon concentration on the bacterial regrowth, repeated experiments were performed using glucose at 0.01 g L^{-1} and 1.0 g L^{-1}, respectively. Fig. 8 shows that the glucose at 0.01 g L^{-1} (ca. COD 16 mg L^{-1}) was rapidly degraded and resulted in a significant COD reduction down to approximately 1 mg COD L^{-1} in 120 min. When *E. coli* was enumerated after the 24 h dark period, the bacterial regrowth was suppressed. Similar glucose degradation was observed after 120 min at an initial glucose concentration of 1.0 g L^{-1}. A significant bacterial regrowth, however, was found to be associated with a high glucose concentration. Therefore, it could be concluded that COD content of the targeted water could affect significantly on the inactivation activity and the BRP of the treated water. Ultimately, the irradiation time required for a successful operation of the photocatalytic treatment process needs to be justified according to the chemical compositions and contents of the target water.

4. Conclusion

The photocatalytic inactivation of sewage isolated *E. coli* strain (ATCC 11775) using TNC was successfully implemented in this study. Under UVA irradiation, the 99.999% inactivation level of 7×10^6 CFU mL^{-1} *E. coli* was well-attained within 60 min in the ASP system operated under the optimal operating conditions: TNC of 1 g L^{-1}, pH 4.0–5.0 and aeration rate of 5 L min^{-1}. The log-linear rate constant, k_2, derived from the modified Hom model suggested that the photocatalytic inactivation activity using the TNC is comparable to the commercial Degussa P25 TiO_2. We found that the Fe^{2+} at 1.0 mg L^{-1} could induce RDE during the post-irradiation period, but will prolong the total irradiation time required. Simple organic carbon, such as glucose can be photocatalyzed into other intermediate forms, while *E. coli* was preferentially oxidized in the 120 min photocatalytic treatment. The persistent intermediate carbon forms were seen as the synergistic factor that affects the biostability of the treated water to bacterial regrowth. It is thus anticipated that the COD of the targeted water needs to be low, in order to functionalize the TNC-ASP system as a potential advanced wastewater treatment process.

Acknowledgements

The authors would like to thank Mr. Philip Adcock for his valuable discussions and feedback during the initial planning stage of this study. This work was funded by the Australian Research Council Linkage Grant (LP0562153) and the Australian Water Quality Centre, SA Water Corporation through the Water Environmental Biotechnology Laboratory (WEBL) at the University of Adelaide.

References

[1] L. Rizzo, J. Koch, V. Belgiorno, M.A. Anderson, Desalination 211 (2007) 1–9.
[2] S.R. Couto, A. Dominguez, A. Sanroman, Chemosphere 46 (2002) 83–86.
[3] J.H. Jeon, S.D. Kim, T.H. Lim, D.H. Lee, Chemosphere 60 (2005) 1162–1168.
[4] W.L. Kostedt IV, J. Drwiega, D.W. Mazyck, S.W. Lee, C.Y. Wu, P. Chadik, Environ. Sci. Technol. 39 (2005) 8052–8056.
[5] M.N. Chong, S. Lei, B. Jin, C. Saint, C.W.K. Chow, Sep. Purif. Technol. 67 (2009) 355–363.
[6] C.S. Zalazar, C.A. Martin, A.E. Cassano, Chem. Eng. Sci. 60 (2005) 4311–4322.
[7] A.P. Toor, A. Verma, C.K. Jotshi, P.K. Bajpai, V. Singh, Dyes Pigments 68 (2006) 53–60.
[8] I.J. Ochuma, R.P. Fishwick, J. Wood, J.M. Winterbottom, Appl. Catal. B: Environ. 73 (2007) 259–268.
[9] J.M. Herrmann, Catal. Today 53 (1999) 115–129.
[10] I.K. Konstantinou, T.A. Albanis, Appl. Catal. B: Environ. 49 (2004) 1–14.
[11] R.J. Watts, S. Kong, W. Lee, J. Environ. Eng. 121 (1995) 730–735.
[12] P.S.M. Dunlop, J.A. Byrne, N. Manga, B.R. Eggins, J. Photochem. Photobiol. A: Chem. 148 (2002) 355–363.
[13] J. Marugán, R. van Grieken, C. Sordo, C. Cruz, Appl. Catal. B: Environ. 82 (2008) 27–36.
[14] H.M. Coleman, C.P. Marquis, J.A. Scott, S.S. Chin, R. Amal, Chem. Eng. J. 113 (2005) 55–63.
[15] J. Wist, J. Sanabria, C. Dierolf, W. Torres, C. Pulgarin, J. Photochem. Photobiol. A: Chem. 147 (2002) 241–246.
[16] A.G. Rincón, C. Pulgarin, Appl. Catal. B: Environ. 63 (2006) 222–231.
[17] T. Matsunaga, R. Tomodam, T. Nakajima, H. Wake, FEMS Microbiol. Lett. 29 (1985) 211–214.
[18] E.J. Wolfrum, J. Huang, D.M. Blake, P.C. Maness, Z. Huang, J. Fiest, Environ. Sci. Technol. 36 (2002) 3412–3419.
[19] J. Hong, M. Otaki, J. Biosci. Bioeng. 96 (2003) 298–303.
[20] J.A. Ibáñez, M.I. Litter, R.A. Pizarro, J. Photochem. Photobiol. A: Chem. 157 (2003) 81–85.
[21] A. Arques, A.M. Amat, L.S. Juanes, R.F. Vercher, M.L. Marin, M.A. Miranda, J. Mol. Catal. A: Chem. 271 (2007) 221–226.
[22] D. Beydoun, R. Amal, Mater. Sci. Eng. B 94 (2002) 71–81.
[23] A. Bhattacharyya, S. Kawi, M.B. Ray, Catal. Today 98 (2004) 431–439.
[24] Z. Ding, H.Y. Zhu, G.Q. Lu, P.F. Greenfield, J. Colloid Interface Sci. 209 (1998) 193–199.
[25] J. Fernandez, J. Kiwi, J. Baeza, J. Freer, C. Lizama, H.D. Mansilla, Appl. Catal. B: Environ. 48 (2004) 205–211.
[26] K. Mogyorosi, I. Dekany, J.H. Fendler, Langmuir 19 (2003) 2938–2946.
[27] R. Molinari, F. Pirillo, M. Falco, V. Loddo, L. Palmisano, Chem. Eng. Proc. 43 (2004) 1103–1114.
[28] S. Takeda, S. Suzuki, H. Odaka, H. Hosono, Thin Solid Films 392 (2001) 338–344.
[29] Z. Xiong, Y. Xu, L. Zhu, J. Zhao, Langmuir 21 (2005) 10602–10607.
[30] W. Yan, B. Chen, S.M. Mahurin, E.W. Hagaman, S. Dai, H. Overbury, J. Phys. Chem. B 108 (2004) 2793–2796.
[31] M.N. Chong, V. Vimonses, S. Lei, B. Jin, C. Chow, C. Saint, Microporous Mesoporous Mater. 117 (2009) 233–242.
[32] A.G. Rincón, C. Pulgarin, Appl. Catal. B: Environ. 49 (2004) 99–112.
[33] A.G. Rincón, C. Pulgarin, Catal. Today 101 (2005) 331–344.
[34] J.A. Herrera Melián, J.M. Doña Rodríguez, A. Viera Suárez, E. Tello Rendón, C. Valdés do Campo, J. Arana, J. Pérez Peña, Chemosphere 41 (2000) 323–327.
[35] M.N. Chong, B. Jin, H.Y. Zhu, C.W.K. Chow, C. Saint, Chem. Eng. J. 150 (2009) 49–54.
[36] H. Zhu, X. Gao, Y. Lan, D. Song, Y. Xi, J. Zhao, J. Am. Chem. Soc. 126 (2004) 8380–8381.
[37] H.Y. Zhu, Y. Lan, X.P. Gao, S.P. Ringer, Z.F. Zheng, D.Y. Song, J.C. Zhao, J. Am. Chem. Soc. 127 (2005) 6730–6736.
[38] APAH, Standard Methods for the Examination of Water and Wastewater, 21st edition, 2005.
[39] A.G. Rincón, C. Pulgarin, Appl. Catal. B: Environ. 44 (2003) 263–284.
[40] A.G. Rincón, C. Pulgarin, Appl. Catal. B: Environ. 51 (2004) 283–302.
[41] Q. Chang, H. He, Z. Ma, J. Inorg. Biochem. 102 (2008) 1736–1742.
[42] R. Sonohara, N. Muramatsu, H. Ohshima, T. Kondo, Biophys. Chem. 55 (1995) 273–277.
[43] M. Heyde, R. Portalier, FEMS Microbiol. Lett. 69 (1990) 19.
[44] H.N. Pham, T. McDowell, E. Wilkins, J. Environ. Sci. Health A 30 (1995) 627–636.
[45] R.J.W. Lambert, M.D. Johnston, E.A. Simons, J. Appl. Microbiol. 87 (1999) 782–786.
[46] R.J.W. Lambert, M.D. Johnston, J. Appl. Microbiol. 88 (2000) 907–913.
[47] M. Cho, H. Chung, W. Choi, J. Yoon, Water Res. 38 (2004) 1069–1077.
[48] M. Cho, H. Chung, J. Yoon, Appl. Environ. Microbiol. 69 (2003) 2284–2291.
[49] L.L. Gyürék, G.R. Finch, J. Environ. Eng. 124 (1998) 783–792.
[50] A.K. Benabbou, Z. Derriche, C. Felix, P. Lejeune, C. Guillard, Appl. Catal. B: Environ. 76 (2007) 257–263.
[51] S.B. Farr, T. Kogoma, Microbiol. Rev. 55 (1991) 561–585.
[52] R. Dillert, U. Siemon, D. Bahnemann, Chem. Eng. Technol. 21 (1998) 356–358.
[53] I.C. Escobar, S. Hong, A.A. Randall, J. Membr. Sci. 175 (2000) 1–17.
[54] F. Ribas, J. Frías, J.M. Huguet, F. Lucena, Water Res. 31 (1997) 639–649.
[55] I.C. Escobar, A.A. Randall, Water Res. 35 (2001) 4444–4454.